

Fluorescence X-ray absorption spectroscopy using a Ge pixel array detector: application to high-temperature superconducting thin-film single crystals

H. Oyanagi,^{a*} A. Tsukada,^{b‡} M. Naito,^{b‡} N. L. Saini,^c M.-O. Lampert,^d
D. Gutknecht,^d P. Dressler,^d S. Ogawa,^e K. Kasai,^f S. Mohamed^{a¶} and A. Fukano^a

^aNational Institute of Advanced Industrial Science and Technology, 1-1-1 Umezono, Tsukuba 305-8568, Japan, ^bNTT Basic Research Laboratories, 3-1 Morinosato-Wakamiya, Atsugi, Kanagawa 243-0198, Japan, ^cUniversita di Roma 'La Sapienza', P. le Aldo Moro 2, 00185 Roma, Italy, ^dCanberra-Eurisys SA, 1 Chemin de la Roserate Lingolsheim, 67834 Tanneries CEDEX, France, ^eOgawa Consulting Engineer's Office, 217 Famile Villa Gotennban Hihashitanaka, 1417-2 Gotennba, Shizuoka 417-0026, Japan, and ^fNE Software, 9-3 Wakaba, Kakizaki-cho, Inashiki-gun, Ibaraki 300-1249, Japan. E-mail: h.oyanagi@aist.go.jp

A Ge pixel array detector with 100 segments was applied to fluorescence X-ray absorption spectroscopy, probing the local structure of high-temperature superconducting thin-film single crystals (100 nm in thickness). Independent monitoring of pixel signals allows real-time inspection of artifacts owing to substrate diffractions. By optimizing the grazing-incidence angle θ and adjusting the azimuthal angle φ , smooth extended X-ray absorption fine structure (EXAFS) oscillations were obtained for strained (La,Sr)₂CuO₄ thin-film single crystals grown by molecular beam epitaxy. The results of EXAFS data analysis show that the local structure (CuO₆ octahedron) in (La,Sr)₂CuO₄ thin films grown on LaSrAlO₄ and SrTiO₃ substrates is uniaxially distorted changing the tetragonality by $\sim 5 \times 10^{-3}$ in accordance with the crystallographic lattice mismatch. It is demonstrated that the local structure of thin-film single crystals can be probed with high accuracy at low temperature without interference from substrates.

© 2006 International Union of Crystallography
Printed in Great Britain – all rights reserved

Keywords: pixel array detector; fluorescence XAS; high-temperature superconductivity; thin-film single crystals.

1. Introduction

Strong coupling between electrons and lattice vibrations (phonons) in high-temperature superconducting (HTSC) materials was recently demonstrated by angle-resolved photoemission spectroscopy (Lanzara *et al.*, 2001). X-ray absorption spectroscopy (XAS) is a powerful local probe which reveals the local displacement of O atoms as carriers are doped (Bianconi *et al.*, 1996), indicating an intimate relationship between lattice effects and the pairing mechanism. Direct observation of isotope (Khasanov *et al.*, 2004) and strain (pressure) (Gao *et al.*, 1994) effects are considered to establish the role of the lattice in HTSC. For instance, under epitaxial strain *T*-(La,Sr)₂CuO₄ (LSCO) thin-film single crystals exhibit significant strain dependence on the superconducting critical

temperature and metallic transport properties (Sato & Naito, 1997; Locquet *et al.*, 1998; Bozoić *et al.*, 2002).

In order to probe the local lattice of thin-film single crystals, a highly sensitive XAS technique is needed, but minimizing the contribution of substrates is also important as these thin films are epitaxially grown on thick single-crystal substrates. Fluorescence detection in a grazing-incidence geometry (Heald *et al.*, 1984) dramatically improves the surface sensitivity. Rapid and sensitive measurements of surface-sensitive XAS became feasible by combining a surface-sensitive geometry and a high-efficiency detector [such as a dense-packed solid-state detector (SSD) array] (Oyanagi *et al.*, 1995), providing a submonolayer surface sensitivity of the order of 10^{14} cm⁻².

Various types of multi-element SSD arrays have been designed and built (Cramer *et al.*, 1988; Oyanagi *et al.*, 1998; Farrow *et al.*, 1994). A pixel array detector (PAD) is a novel approach to overcoming mechanical limitations in the close packing of independent SSD elements. The basic specifica-

[‡] Present address: Tokyo University of Agriculture and Technology, 2-24-6 Nakacho, Koganei-shi, Tokyo 184-8588, Japan.

[¶] Present address: Venture Business Laboratory, Nagoya University, Furocho, Chigusa-ku, Nagoya 464-8601, Japan.

tions and performance of a Ge PAD have been reported elsewhere (Oyanagi *et al.*, 2002). Here we describe the electronics, *i.e.* a high-density analog–digital ‘hybrid’ CAMAC module, and the result of an application to an XAS study of LSCO thin-film single crystals under strain. Using a segmented X-ray detector is a practical method of increasing the total throughput, keeping a linear response, but it is also useful for improving the systematic (non-statistical) error. The latter, in the case of thin films, is achieved by monitoring strong diffractions from substrates and rearranging the sample geometry. The PAD used in the current experiment is a monolithic array achieving almost 100% packing density. Each pixel is separated by 0.3 mm. Note that modern high-energy photon sources (6–8 GeV) require a detector efficiency over a wide energy range (5–60 keV), for which germanium is ideal.

2. Experimental

2.1. PAD electronics

The PAD used in this work consists of a 10×10 array of Ge pixels ($4.7 \text{ mm} \times 4.7 \text{ mm}$) of thickness $t = 7.5 \text{ mm}$. Fig. 1 illustrates the PAD data-acquisition (DAC) system. Each pixel output is fed into a separate analog preamplifier board. The PSC 854 preamplifier consists of two components: (i) an input circuit contained in the cryostat and cooled to a temperature slightly higher than 77 K, including the field-effect transistor, feedback resistor and feedback capacitor; (ii) an external part containing the main board which processes the input pulses. Preamplifier output for each channel is fed into one of the linear input channels of the analog–digital hybrid CAMAC module (eight channels per two-span module) and the pulse

heights of all 100 outputs are independently analyzed. A total of 13 CAMAC modules are controlled using a linux PC through two SCSI CAMAC controllers (Model 73A SCSI Bus Crate Controller, Jorway). Two linux PCs are connected by ethernet and recorded data are displayed in a data-acquisition (DAC) PC (Dimension 8250, DELL) while another PC (Dimension 8300, DELL) is used for EXAFS data analysis. One of the 13 hybrid CAMAC modules accepts transistor–transistor level (TTL) output pulses from digitized ion chambers used as the incident-beam and reflected-beam intensity monitors. The reflected-beam monitor is used in setting up the total reflection geometry, giving the highest surface sensitivity. To scan the photon energy, a double-crystal monochromator (Oyanagi *et al.*, 1996) is controlled by a DAC software (C/linux).

The energy resolution of the PAD was determined for each channel from the full width at half-maximum (FWHM) of the Mn $K\alpha$ peak (5.9 keV) using a standard source (^{55}Fe). The average energy resolution with a time constant of $0.5 \mu\text{s}$ was 245 eV. Amplifier dead-time degrades throughput owing to pulse pile-up. We evaluated the amplifier throughput for each channel from the non-linearity of the detector output rate. The hybrid PAD electronics output starts to deviate from a linear function for input count rates greater than $10 \text{ kcounts s}^{-1}$. Even with a fast shaping time ($0.5 \mu\text{s}$), corrections to non-linearity caused by dead-time are needed. Standard correction formulae seem to be valid for input count rates less than $100 \text{ kcounts s}^{-1}$. After a dead-time correction on a DAC PC, a linear response is obtained below the maximum count rate ($100 \text{ kcounts s}^{-1}$). The total maximum count rate is thus $\sim 10 \text{ MHz}$. The maximum throughput is limited by both analog (amplifier dead-time) and digital (single-channel

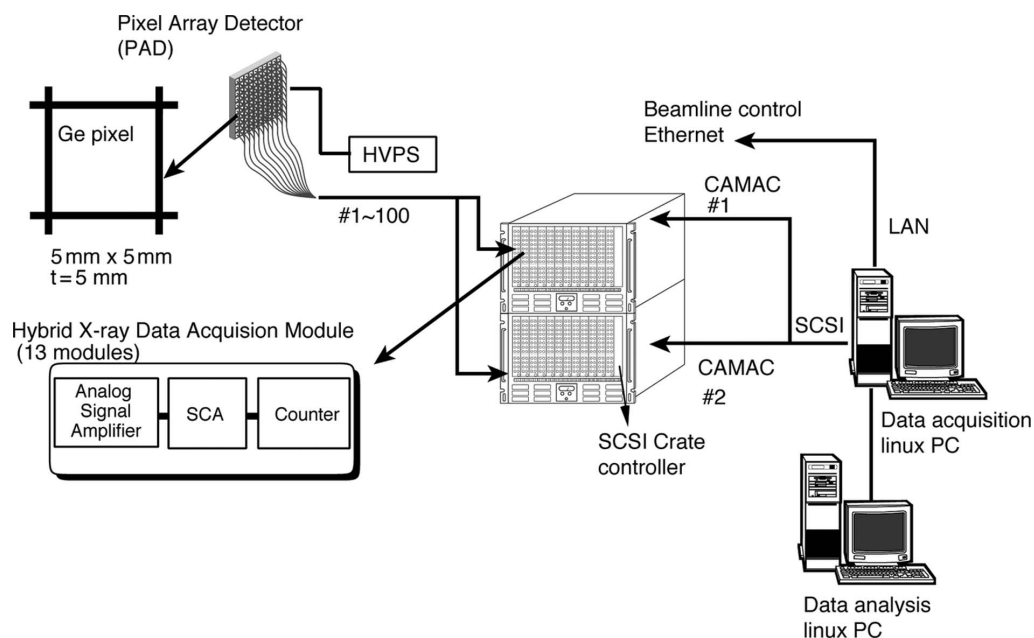


Figure 1

Schematic of the hybrid electronics and data-acquisition system. Each CAMAC module has four independent analog circuits (spectroscopy amplifier) and digital circuits (single-channel analyzers and counters) controlled by a SCSI CAMAC controller. The data-acquisition system consists of two ethernet-connected linux PCs.

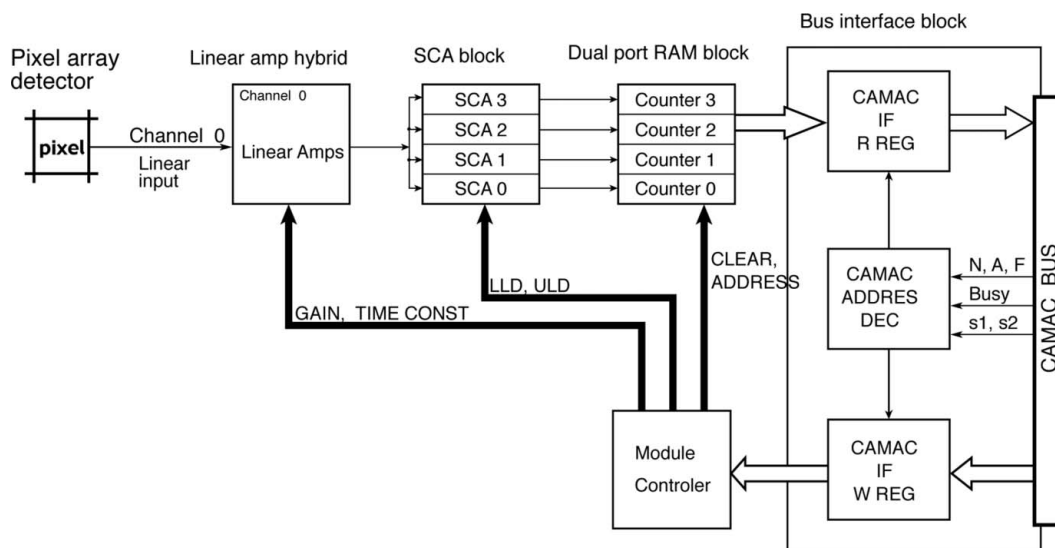


Figure 2 Block diagram of the hybrid electronics (double-width CAMAC module). Analog parameters of a linear amplifier are downloaded from data-acquisition software on a linux PC. The output of the amplifier is fed into a SCA block which analyzes the pulse height of the signal, and the intensity of eight independent regions of interest is recorded in the memory.

analyzer and memory) circuits. A digital signal processor would improve the total throughput to 50–100 MHz (Warburton *et al.*, 1996). In order to simplify the setting procedures of the electronics, we adopted a ‘hybrid’ approach. In the present experiment a typical input count rate per pixel for a 100 nm-thick LSCO thin-film single crystal was ~ 10 – 15 kcounts s^{-1} , which guaranteed a linear response in fluorescence yield measurements.

Fig. 2 shows a block diagram of the hybrid CAMAC module. A double-width CAMAC module contains eight linear amplifiers, 32 single-channel analyzers (SCAs), counters, memories, CAMAC bus interfaces and module control circuits. A linear amplifier is composed on a 50 mm \times 60 mm sub-board, as shown in Fig. 3. It has a sixth-order Gaussian filter. Amplifier gain is adjustable between 25 and 200 and the time constant can be selected from 0.5, 1 and 3 μs . These parameters are controlled by data-acquisition software (C/linux) and referred to as a database. Below the amplifier sub-board are installed four SCA boards. The lower discrimination levels (LLDs) and the window widths of the SCAs are set up digitally by the DAC PC. The resolution of the LLD and SCA window width are 12 bits and 8 bits, respectively. Each SCA channel has a 24-bit counter and four independent memories. Because four memories per SCA channel are provided, we can acquire four sequential data sets without latency. This allows us to monitor fluorescence lines of interests and those for internal reference (intensity monitor). Parameters controlling the amplifiers and SCAs are downloaded into a CAMAC module from the database and there is no need to adjust them. A microprocessor (Hitachi H8/3048) is used as a module controller. For timing, the gate signal and memory numbers are fed through an independent connector disposed on the back plane. These signals precisely control the timing and memory allocations in the circuits since latency of the

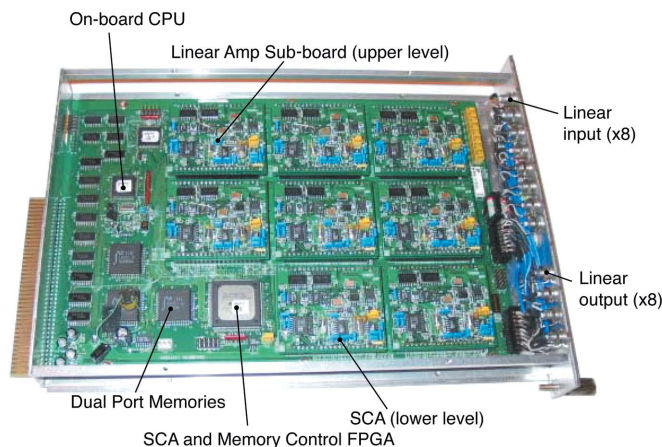


Figure 3 Side view of the hybrid CAMAC module. The locations of the major components (functions) are shown. To achieve a dense packing, the linear amplifier sub-board and SCA sub-board are stacked. An on-board CPU (Hitachi H8), dual port memories and a field programmable gate array (FPGA) for controlling the SCA and memories are indicated.

CAMAC bus cannot be neglected when simultaneously controlling 13 modules.

2.2. XAS experiment

In Fig. 4(a) our experimental XAS set-up at BL13B of the Photon Factory is schematically illustrated. The sample (10 mm \times 10 mm) is mounted on an aluminium holder using strain-free glue (G4) and attached to a closed-cycle helium refrigerator which rotates on a high-precision goniometer (Huber 420) to change the incidence angle. Samples are 100 nm-thick LSCO grown on LaSrAlO₄ (LSAO) and SrTiO₃ (STO) (Naito & Sato, 1995). The fluorescence signal is recorded over a cone-like solid angle perpendicular to the

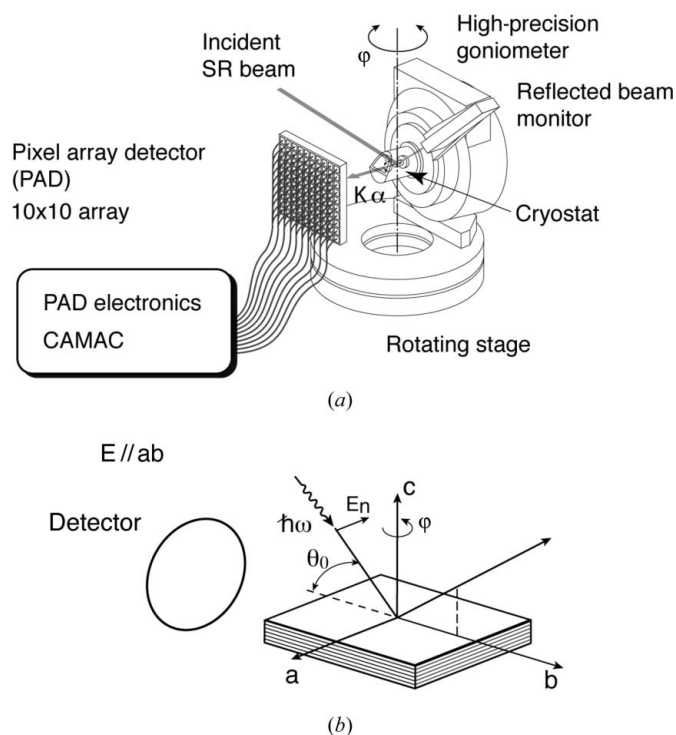


Figure 4

Schematic of the XAS set-up in fluorescence mode. A PAD consisting of a 10×10 array of a germanium pn junction is used to record fluorescence as a monochromatic synchrotron radiation beam excites elements in a sample mounted on a cryostat. Output signals of the PAD are fed into analog–digital hybrid electronics and analyzed.

incident beam and away from scattering plane as illustrated in Fig. 4(b). This arrangement was used to measure EXAFS with the electric field vector \mathbf{E} parallel to the ab plane ($\mathbf{E} // ab$), while the sample is rotated by 90° for probing along the c -axis ($\mathbf{E} // c$). Details of the experiments are described elsewhere (Oyanagi, 1998).

Thin films of LSCO single-crystal were grown in a molecular beam epitaxy chamber from metal sources using multiple electron-gun evaporators with accurate stoichiometry control of the atomic beam fluxes (Tsukada *et al.*, 2002). The samples were grown on LSAO and STO substrates ($10 \text{ mm} \times 10 \text{ mm}$). The temperature dependence of the resistivity, measured using a four-probe method, showed superconductivity at a higher temperature than that of the bulk single-crystal by $\sim 24\%$ ($T_c = 43.4 \text{ K}$ with $\Delta T < 1.0 \text{ K}$) for the LSAO substrate, and at a lower temperature by $\sim 46\%$ ($T_c = 19 \text{ K}$ with $\Delta T < 9.0 \text{ K}$) for the STO substrate. The oxygen concentration was carefully controlled by post-growth oxidation by ozone gas annealing. The lattice parameters of the thin films were obtained from X-ray diffraction patterns.

All XAS measurements were performed in fluorescence detection mode at BL13B of the Photon Factory. The energy and maximum electron current were 2.5 GeV and 400–450 mA, respectively. A directly water-cooled silicon (111) double-crystal monochromator (Oyanagi *et al.*, 1996) was used, covering the energy range between 4 keV and 25 keV. The energy resolution was better than 2 eV at 9 keV, cali-

brated from the near-edge features of copper metal at the Fermi energy (E_f) (8.9803 keV). Careful alignment of the sample geometry on a precision goniometer was repeated until artifacts were not present in the region of interest. The sample was attached to an aluminium holder with a strain-free glue and cooled using a closed-cycle He refrigerator (cooling power: 2 W at 20 K; stability: $\pm 0.1 \text{ K}$).

3. Results and discussion

3.1. Data analysis

Fluorescence yield spectra were obtained by integrating 100 channels giving a total count of 2.4×10^7 counts per data point. Each data point was integrated for 4 s, and five independent scans were repeated in order to minimize systematic error. Fig. 5 shows the raw Cu $K\alpha$ fluorescence yield as a function of photon energy measured for 100 nm-thick LSCO grown on LSAO with $\theta = 10^\circ$, 5° and 1° . It can be seen that with the decrease of incidence angle the effect of substrate diffraction is reduced, and with $\theta = 1^\circ$ the artifact is not observed.

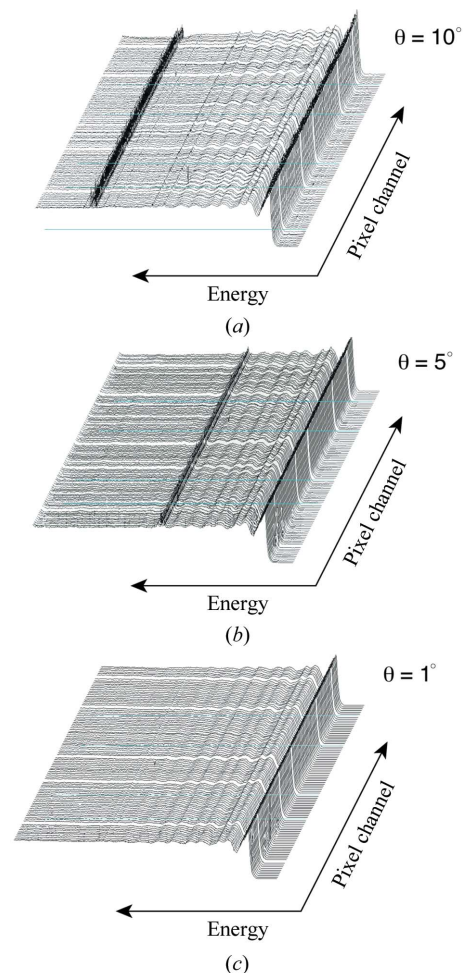
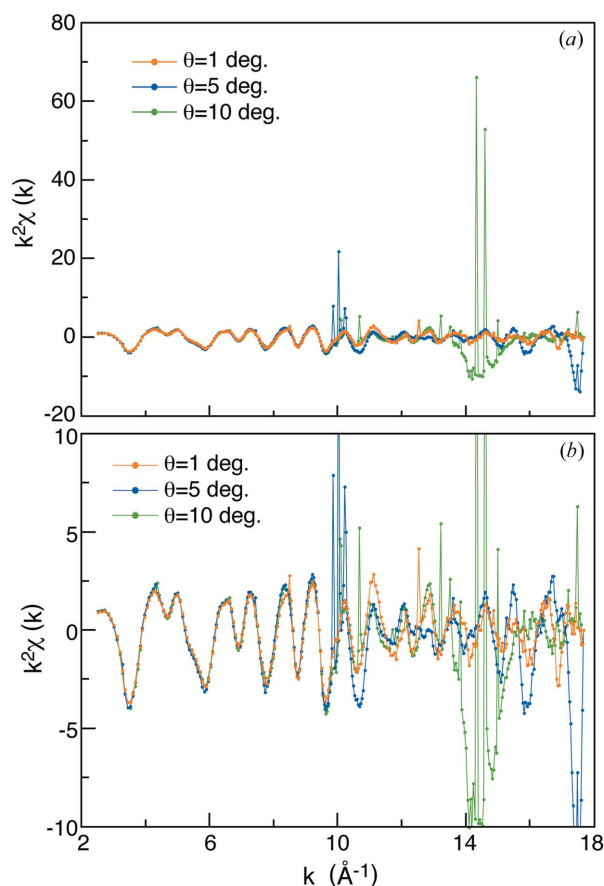


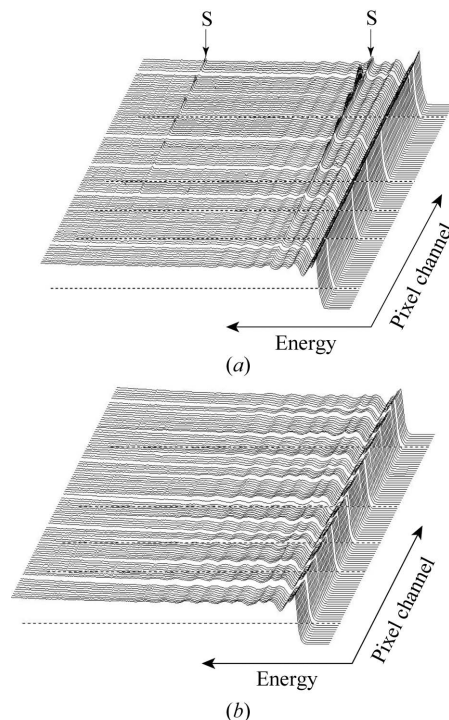
Figure 5

Raw Cu $K\alpha$ fluorescence yield as a function of photon energy measured for 100 nm-thick LSCO grown on LSAO with (a) $\theta = 10^\circ$, (b) $\theta = 5^\circ$ and (c) $\theta = 1^\circ$.


Figure 6

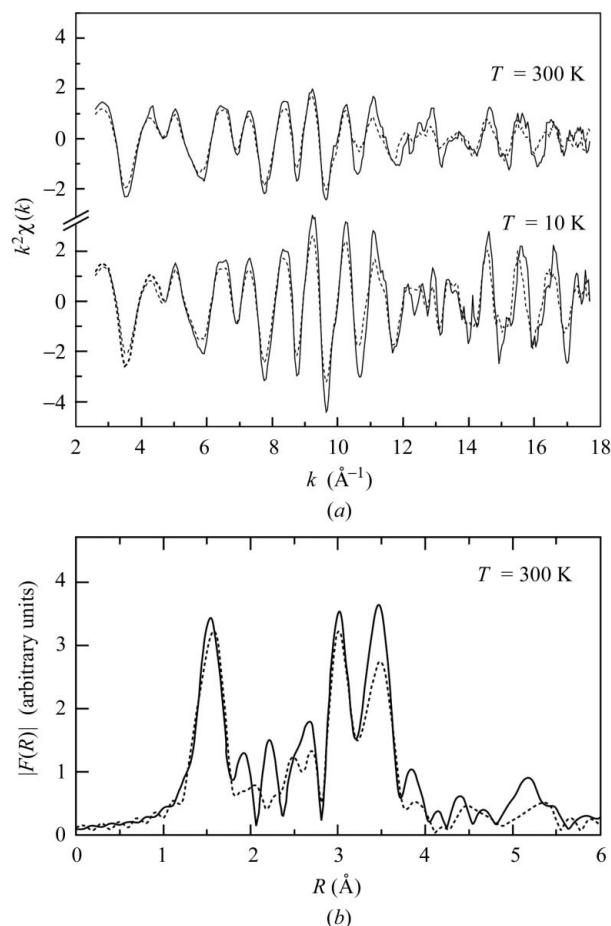
(a) Normalized EXAFS oscillations for 100 nm-thick LSCO grown on LSAO substrate with various incidence angles θ . Anomalies (sharp peaks and wiggles) are obvious for geometries with $\theta = 5^\circ$ and $\theta = 10^\circ$. By choosing an optimum angle of incidence for 100 nm thickness, artifacts are suppressed. (b) Expanded plot of the same data.

Fig. 6(a) shows the normalized in-plane polarized Cu K -EXAFS oscillations for LSCO thin-film single-crystal ($x = 0.15$) grown on LSAO substrates, hereafter referred to as LSCO/LSAO, as a function of the photoelectron wavenumber k . Closed circles and solid curves indicate the EXAFS data taken at 300 K with different incidence angles. Sharp peaks (artifacts due to substrate diffractions) are evident in the EXAFS data around 10 \AA^{-1} and 14 \AA^{-1} when $\theta = 5^\circ$ and 10° , respectively. As shown in the same plot with an expanded vertical scale (Fig. 6b), artifacts become less clear as the incidence angle is decreased, and with $\theta = 1^\circ$ most of the diffraction effects disappear. These results demonstrate that grazing-incidence geometry dramatically suppresses the effect of substrate diffractions. The geometry is further optimized by azimuthal rotation of the sample, monitoring PAD outputs as the photon energy is scanned. Fig. 7(a) shows the raw fluorescence yield spectra after normalizing by the incident-beam intensity. The arrows marked with an S indicate artifacts arising from substrate diffractions, which disappear as the azimuthal angle is rotated (Fig. 7b). Employing a PAD is quite useful for monitoring the solid angle of the segmented detector and adjusting the geometry.


Figure 7

(a) Raw Cu $K\alpha$ fluorescence yield as a function of photon energy measured for 100 nm-thick LSCO grown on LSAO with $\theta = 1^\circ$. Above the absorption edge, position-dependent artifacts (indicated by the arrows marked with an S) due to scattering from substrates are observed. (b) The same measurement after azimuthal rotation.

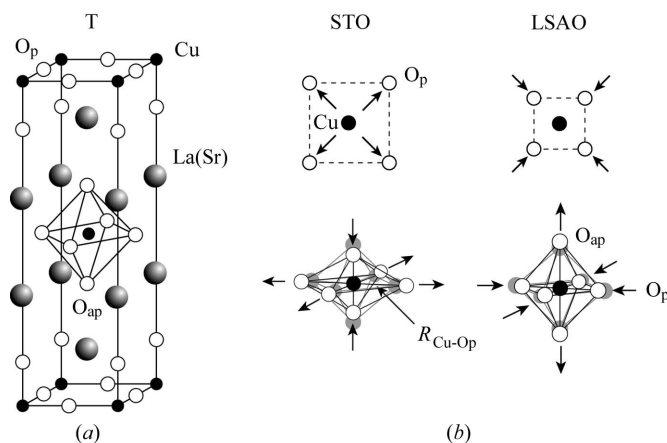
In Fig. 8(a) the optimized EXAFS oscillations for LSCO/LSAO taken at 300 K and 10 K are shown. The solid and dashed lines indicate the results for thin film and bulk single crystals, respectively. The amplitude of the latter data is reduced by the effect of self-absorption. The k -dependent profile of the total oscillations reflects the weighted sum of the scattering amplitude functions of La(Sr), Cu and O. Individual EXAFS data ($k < 16 \text{ \AA}^{-1}$) for the nearest-neighbor Cu–O_p (where O_p is an in-plane O atom) and next-nearest neighbor Cu–Cu correlations are filtered and curve-fitted in k -space using a single-scattering formula. Fig. 8(b) shows the Fourier transform (FT) magnitude curves for the 300 K data of Fig. 8(a). Three prominent peaks correspond to the Cu–O_p, Cu–La(Sr) and Cu–Cu correlations. The prominent peak in the FT magnitude at $R \approx 1.5 \text{ \AA}$ is the nearest-neighbor Cu–O_p. The theory curves are calculated from a single-scattering formula and theoretical phase-shift functions using *FEFF7* (Rehr *et al.*, 1992). Structural parameters such as the in-plane Cu–O_p distance $R_{\text{Cu-O}_p}$ and mean-square relative displacement of O atoms $\sigma_{\text{Cu-O}_p}$ relative to copper ions are determined by least-squares curve fitting in k -space. The determined $R_{\text{Cu-O}_p}$ values for thin-film LSCO/LSAO and LSCO/STO are $1.88 \pm 0.01 \text{ \AA}$ and $1.90 \pm 0.01 \text{ \AA}$, respectively, in agreement with the crystallographic values, $a_0/2$, determined by X-ray diffraction patterns. Since $R_{\text{Cu-O}_p} = 1.89 \pm 0.01 \text{ \AA}$ in a bulk single crystal (Radaelli *et al.*, 1994), the local oxygen displacement within CuO₂ is $\Delta R_{\text{Cu-O}_p}/R_{\text{Cu-O}_p} \approx 5 \times 10^{-3}$.


Figure 8

(a) Normalized Cu K-EXAFS oscillations for 100 nm-thick LSCO thin film grown on LSAO (solid line) and bulk single-crystal (dashed line). The upper and lower rows indicate the data recorded at 300 K and 10 K, respectively. (b) Magnitude of the complex Fourier transform for the EXAFS curves recorded at 300 K for thin film (solid line) and for a single crystal (dashed line).

3.2. Local structure of LSCO under strain

The crystal structure of LSCO is tetragonal at high temperatures where CuO_6 octahedra are connected to form a square-planar network sharing O atoms (Fig. 9a). Each copper ion is surrounded by four O_p and two apical O atoms (O_{ap}). The CuO_6 octahedron is elongated along the c -axis resulting in two long (2.40 \AA) and four short (1.89 \AA) bonds by Jahn–Teller distortion (Radaelli *et al.*, 1994). The lattice constant a_0 for LSCO/LSAO is 3.758 \AA , smaller than that of optimally doped LSCO ($a_0 = 3.778$ \AA) by 0.02 \AA (or 0.5%). Thus LSCO films grown on LSAO substrate are under compressive strain. Because of strain, the in-plane lattice is shortened while the out-of-plane lattice is expected to increase (the Poisson effect). In contrast, the lattice constant of LSCO/STO ($a_0 = 3.794$ \AA) is larger than that of LSCO by 0.016 \AA (or 0.4%). The epilayer is under tensile strain and the deformation of the lattice is opposite. Our results indicate that in both cases the local displacement of the CuO_6 octahedra is 0.01 \AA (or 0.5%), in agreement with the crystallographic lattice deformation (Fig. 9b).


Figure 9

(a) Crystal structure of a LSCO single crystal. Atomic positions are indicated, *i.e.* copper (black spheres), lanthanum or strontium (large grey spheres) and oxygen (white spheres). (b) In-plane projection (top) and CuO_6 octahedrons (bottom) illustrating deformation due to uniaxial strain.

The advantage of monitoring the segmented solid angle using a PAD is obvious from the EXAFS data for LSCO/LSAO shown in Fig. 8(a), which is free from artifacts and distortions. Least-squares fitting of theoretical curves in k -space for the Cu-O_p and Cu-Cu pairs determined the local structures at any temperature between 300 K and 5.1 K. Although the strain effects we describe here are static in nature and hence temperature-independent, dynamic local distortion arises from the intrinsic instability of hole-doped cuprates below a characteristic temperature T^* (Saini *et al.*, 1997), and a detailed temperature dependence is required.

In this paper we have shown that a PAD is useful in fluorescence XAS experiments on thin-film single crystals. Monitoring the spatial distribution of fluorescence X-rays using a segmented detector such as a PAD can detect artifacts due to substrates. By carefully adjusting the grazing-incidence angle θ and azimuthal orientation angle φ , artifacts due to substrate scattering are easily removed. We have demonstrated that detailed analysis of EXAFS data without artifacts can determine the local structure of strained HTSC single crystals with comparable or even better quality than conventional measurements of bulk materials. Apart from HTSC, thin-film single crystals exhibit interesting properties, such as enhancement of the ferroelectricity (Choi *et al.*, 2004). Local-structure studies will be needed to carefully evaluate the effect of strain, for which the PAD will be a powerful tool.

4. Conclusion

In measurements of thin-film single crystals epitaxially grown on substrates, it is essential to tune the thin layers, minimizing the effect of substrates (scattering, diffraction and standing wave). Grazing-incidence fluorescence geometry can pick up the thin-film information if the angle-dependence of the emitted fluorescence can be monitored in real time. A densely packed pixel array is useful in monitoring the angle-dependence

dence of the fluorescence, distinguishing distortions due to single-crystal substrates. The results of an EXAFS application to high-temperature superconducting cuprate (LSCO) thin-film single crystals (100 nm in thickness) showed that the CuO₆ octahedra are distorted so that the in-plane Cu–O distance is distorted in accordance with the mismatch strain between the epilayer. Fluorescence monitoring using a PAD can be a standard XAS technique of probing the local lattice of thin-film single crystals, avoiding substrate effects.

The authors would like to thank C. Fonne and R. Henck for their contributions to the research and development of the PAD. They express their thanks to J. Mustre de Leon and E. Stern for useful comments and discussions.

References

- Bianconi, A., Saini, N. L., Lanzara, A., Missori, M., Rossetti, T., Oyanagi, H., Yamaguchi, H., Oka, K. & Ito, T. (1996). *Phys. Rev. Lett.* **76**, 3412–3415.
- Bozovic, I., Logvenov, G., Belca, I., Narimbetov, B. & Sveklo, I. (2002). *Phys. Rev. Lett.* **89**, 107001–1–3.
- Choi, K. J., Biegalski, M., Li, Y. L., Sharan, A., Schubert, J., Uecker, R., Reiche, P., Chen, Y. B., Pan, X. Q., Gopalan, V., Chen, L.-Q., Schlom, D. G. & Eom, C. B. (2004). *Science*, **306**, 105–108.
- Cramer, S. P., Tench, O., Yocum, M. & George, G. N. (1988). *Nucl. Instrum. Methods*, **A266**, 586.
- Farrow, R., Derbyshire, G. E., Dobson, B. R., Dent, A. J., Bogg, D., Headspith, J., Lawton, R., Martini, M., Buxton, K. & Trammel, R. (1994). *Physica B*, **208/209**, 256–258.
- Gao, L., Xue, Y. Y., Chen, F., Xiong, Q., Meng, R. L., Ramirez, D., Chu, C. W., Eggert, J. H. & Mao, H. K. (1994). *Phys. Rev. B*, **50**, 4260–4263.
- Heald, S. M., Keller, E. & Stern, E. A. (1984). *Phys. Lett.* **103A**, 155–158.
- Khasanov, R., Eshchenko, D. G., Luetkens, H., Morenzoni, E., Prokscha, T., Suter, A., Garifianov, N., Mali, M., Roos, J., Conder, K. & Keller, H. (2004). *Phys. Rev. Lett.* **92**, 057602–1–4.
- Lanzara, A., Bogdanov, P. V., Zhou, X. J., Keller, S. A., Feng, D. L., Lu, E. D., Yoshida, T., Eisaki, H., Fujimori, A., Kishio, K., Shimoyama, J.-I., Noda, T., Uchida, S., Hussain, Z. & Shen, Z.-X. (2001). *Nature (London)*, **412**, 510–514.
- Locquet, J.-P., Perret, J., Fompeyrine, J., Machler, E., Seo, J. W. & Van Tendeloo, G. (1998). *Nature (London)*, **394**, 453–456.
- Naito, M. & Sato, H. (1995). *Appl. Phys. Lett.* **67**, 2557–2559.
- Oyanagi, H. (1998). *J. Synchrotron Rad.* **5**, 48–53.
- Oyanagi, H., Fonne, C., Gutknecht, D., Dressler, P., Henck, R., Lampert, M.-O., Ogawa, S. & Kasai, K. (2002). *Nucl. Instrum. Methods*, **A513**, 340–344.
- Oyanagi, H., Haga, K. & Kuwahara, Y. (1996). *Rev. Sci. Instrum.* **67**, 350–354.
- Oyanagi, H., Martini, M. & Saito, M. (1998). *Nucl. Instrum. Methods*, **A403**, 58–64.
- Oyanagi, H., Shioda, R., Kuwahara, Y. & Haga, K. (1995). *J. Synchrotron Rad.* **2**, 99–105.
- Radaelli, P. G., Hinks, D. G., Mitchell, A. W., Hunter, B. A., Wagner, J. L., Dabrowski, B., Vandervoort, K. G., Viswanathan, H. K. & Jorgensen, J. D. (1994). *Phys. Rev. B*, **49**, 4163–4175.
- Rehr, J., Zabrinisky, S. I. & Albers, R. C. (1992). *Phys. Rev. Lett.* **69**, 3397–3400.
- Saini, N. L., Lanzara, A., Oyanagi, H., Yamaguchi, H., Oka, K., Itoo, T. & Bianconi, A. (1997). *Phys. Rev. B*, **55**, 12759–12769.
- Sato, H. & Naito, M. H. (1997). *Physica C*, **280**, 178–186.
- Tsukada, A., Greibe, T. & Naito, M. (2002). *Phys. Rev. B*, **66**, 184515–1–5.
- Warburton, W. *et al.* (1996). *Proceedings of the 9th International Conference on X-ray Absorption Fine Structure*, Grenoble, France.